Supporting Information

Sandwich-like multi-scale hierarchical porous carbon with highly hydroxylated surface for flow batteries

Rui Wang[1], Yinshi Li[1,*], Haiying Liu[1], Ya-Ling He[1,*], Mingsheng Hao[1]

[1]Key Laboratory of Thermo-Fluid Science and Engineering of Ministry of Education, School of Energy and Power Engineering, Xi'an Jiaotong University, Xi'an, Shaanxi 710049, China

Fig. S1 Withered platanus leafs in Wutong West Road of Xi'an Jiaotong University.

*Corresponding author.

E-mail addresses: ysli@mail.xjtu.edu.cn (Y. Li)

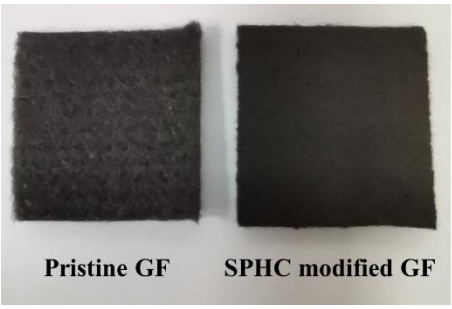

Fig. S2 digital photographs of (a) pristine GF and (b) SPHC modified GF.

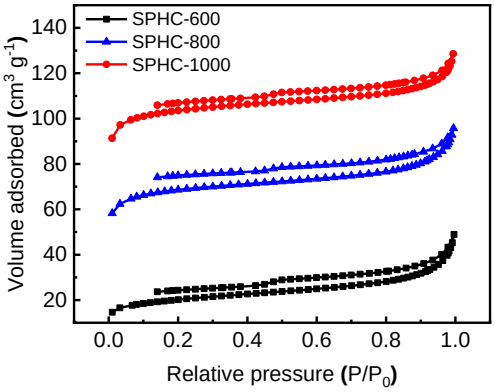

Fig. S3 N_2 adsorption-desorption isotherms of SPHC-600, SPHC-800 and SPHC-1000.

As shown in Fig. S3, a strong adsorption in low pressure region (P/P_0=0-0.1) and an obvious hysteresis loop in medium pressure region (P/P_0=0.4-0.8) for the SPHC-X are respectively attributed to the appearance of the mesopore and micropore. Similar to some biomass-derived carbons[18, 19], it is found that the N_2 adsorption-desorption isotherms of SPHC-X are not closed, which may be caused by the destruction of some pore structures in the N_2 adsorption-desorption process.

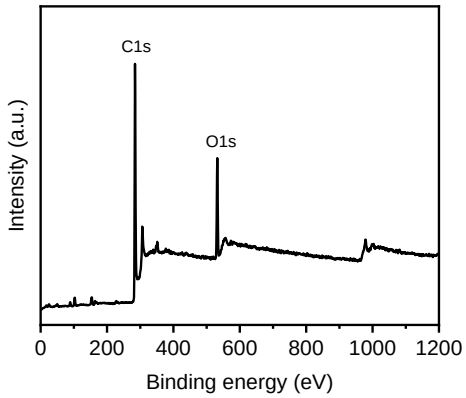

Fig. S4 XPS spectra of the SPHC-1000.

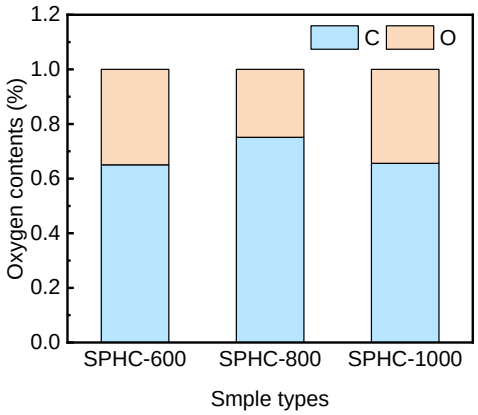

Fig. S5 Chemical composition ratio of oxygen and carbon atoms for SPHC-600, SPHC-800 and SPHC-1000.

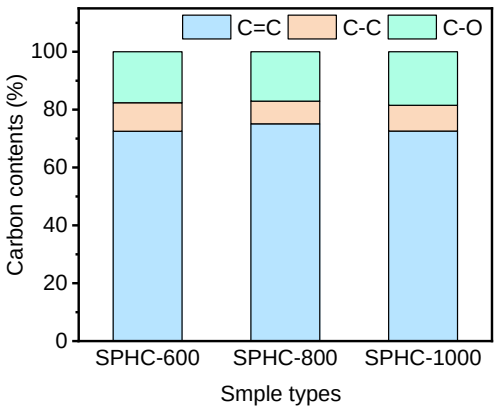

Fig. S6 Chemical composition ratio of SPHC-600, SPHC-800 and SPHC-1000 from C1s spectra.

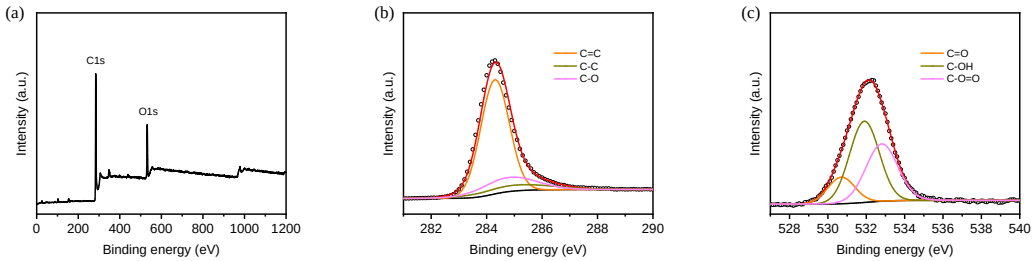

Fig. S7 (a) XPS spectra of the SPHC-600; XPS analysis and its fitting from high resolution (b) C1s peak, (c) O1s peak for SPHC-600.

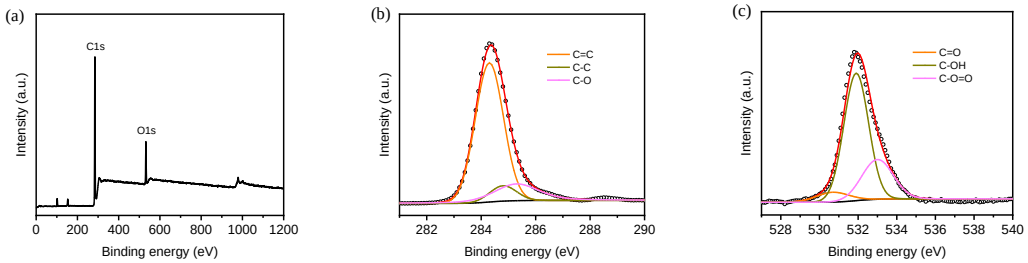

Fig. S8 (a) XPS spectra of the SPHC-800; XPS analysis and its fitting from high resolution (b) C1s peak, (c) O1s peak for SPHC-800.

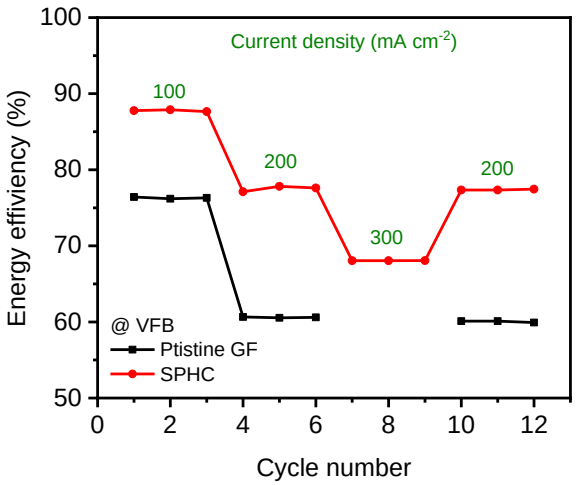

Fig. S9 Energy efficiency of VFBs with pristine GF and SPHC electrodes at different current densities.

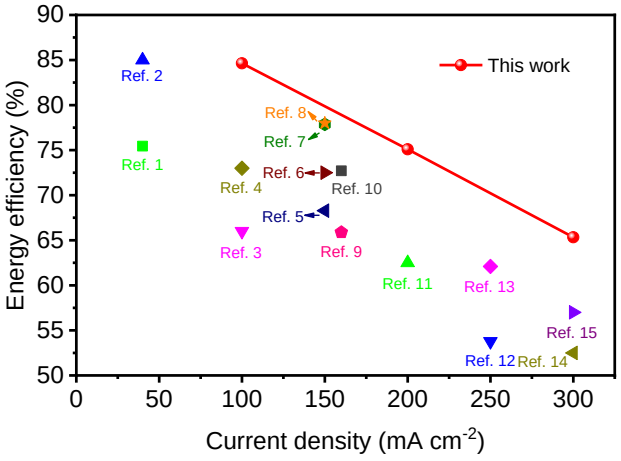

Fig. S10 Performance comparison of VFBs with SPHC electrode, and the VFB performance in the open literature.

Table. S1 Experimantal parameters from the open literature.

Ref.	Sample	electrode size	membrane	electrolyte	flow rate

1	**Wood-derived carbon**	9 cm^2	N115	1.5M	53.4 mL min^{-1}
2	**Lignin-derived carbon**	5.0625 cm^2	N116	1.6M	30 mL min^{-1}
3	**CNF-CNT/GF**	5 cm^2	N117	2.0M	20 mL min^{-1}
4	**Cocoon-derived carbon**	4 cm^2	212	1M	46 mL min^{-1}
5	**Corn-derived carbon**	25 cm^2	N115	2.0M	60 mL min^{-1}
6	**$NiCoO_2$/GF**	4 cm^2	GN-114C	1M	20 mL min^{-1}
7	**rGO/GF**	25 cm^2	N117	3.0M	30 mL min^{-1}
8	**EMIM-coated GF**	4 cm^2	N115	1.6M	20 mL min^{-1}
9	**Nb-WO_3/GF**	10 cm^2	N115	2.0M	20 mL min^{-1}
10	**$TiNb_2O_7$-rGO/GF**	-	-	0.5M	-
11	**P-O-doped GF**	25 cm^2	ACS	1.6m	30 mL min^{-1}
12	**P-F-doped GF**	12 cm^2	N115	1.5M	20 mL min^{-1}
13	**ZrO_2/GF**	4 cm^2	N211	1.1M	-
14	**Dopamine-coated GF**	4 cm^2	N212	1M	46 mL min^{-1}
15	**FeOOH-actived GF**	4 cm^2	N115	0.75M	-

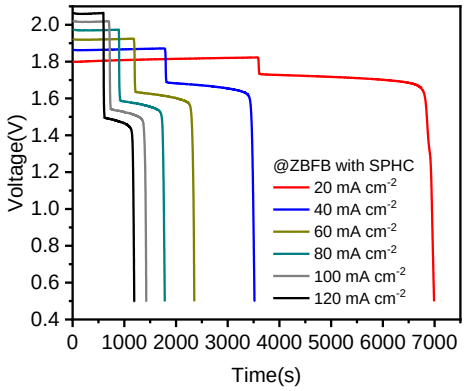

Fig. S11 Charge-discharge curves for ZBFBs with SPHC electrode.

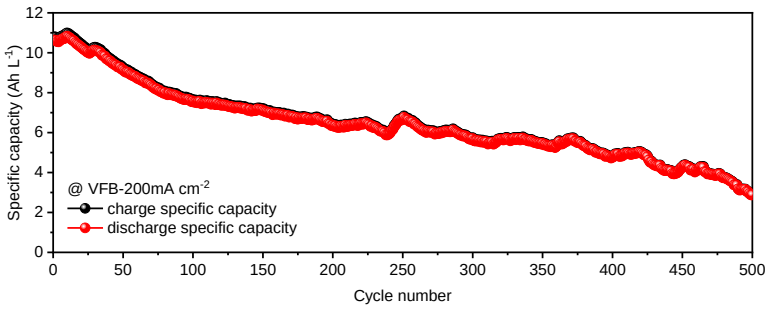

Fig. S12 Capacities during cycling test for VFBs with SPHC at 200 mA cm^{-2}.

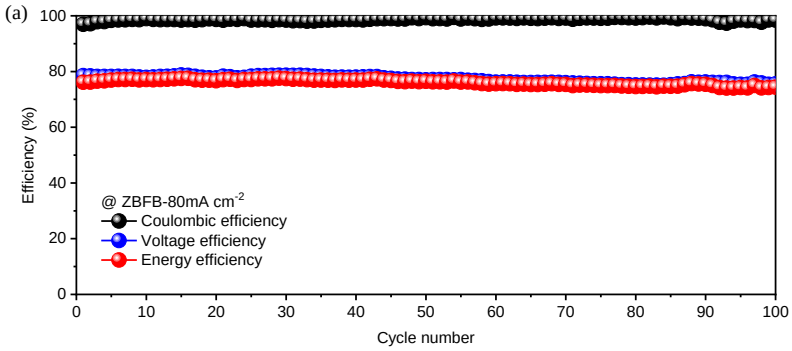

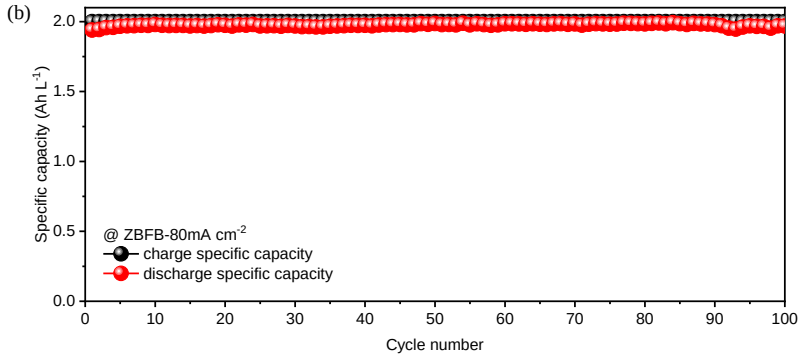

Fig. S13 (a) Efficiencies and (b) capacities during cycling test for ZBFBs with SPHC at 80 mA cm^{-2}.

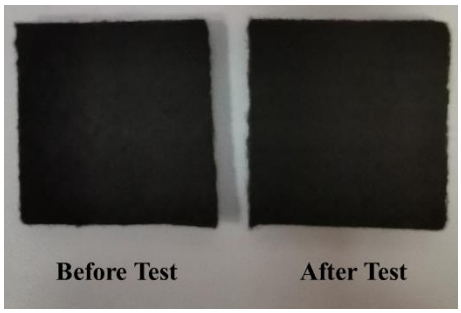

Fig. S14 digital photographs of SPHC-GF electrodes (a) before and after cycling charge-discharge test.

Computational method

Two kinds of porous computational domains in flow battery were investigated by numerical method. Porous materials in different regions were illustrated in Fig. S14. The simulation was carried at the electrode scale and catalyst scale, respectively. First, simulate the flow of the porous medium that fits the flow channel to obtain the flow velocity in the porous medium. Second, further study the flow in secondary pores in porous media. The basic design

parameters and operation conditions are shown in Table 1.

1. Assumptions

(1) The flow battery operates in steady state

(2) Flow in all areas is considered as laminar flow due to the low velocity

(3) The porous domain is considered to be homogeneous.

2. Conservation equations

The Flows in channel was described by Naiver-Stokes equation:

$$\rho(\vec{u}\cdot\nabla)\vec{u} = \nabla\cdot[-pI + \mu(\nabla\vec{u} + (\nabla\vec{u})^T)]$$

$$\rho\nabla\cdot\vec{u} = 0$$

where ρ, μ, u are density, viscosity and velocity respectively

For the flow in porous domain, Naiver-Stokes equation is replaced by the Brinkman equation which takes into account the porosity correction.

$$\frac{1}{\epsilon}\rho(\vec{u}\cdot\nabla)\vec{u}\frac{1}{\epsilon} = \nabla\cdot[-pI + \frac{\mu}{\epsilon}(\nabla\vec{u} + (\nabla\vec{u})^T)] - \frac{\mu}{k}\vec{u}$$

where ϵ is porosity and k is permeability.

k_0 is known at porosity ϵ_0. When the porosity changes to ϵ, the permeability can be known from the following equation:

$$k = k_0\frac{(1-\epsilon_0)^2}{\epsilon_0^3}\frac{\epsilon^3}{(1-\epsilon)^2}$$

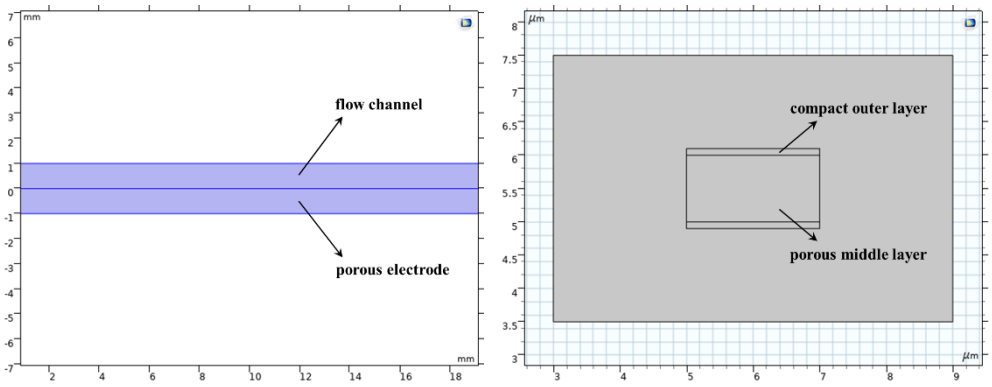

Fig. S15 Computational domains of (a) electrode under flow channel and (b) sandwich-like porous structure.

Table S2 Modeling parameters related to electrode and electrolyte properties.

Parameter	Symbols	Value	Ref.
Electrolyte flow rate	Q_{in}	$46ml\ min^{-1}$	Experiment
Graphite porosity	ϵ_f	0.9	Experiment
Secondary porosity	ϵ_s	0.5	Experiment
Outlet pressure	P_{out}	$1\ atm$	Experiment
Original fluid permeability	k_0	$2 * 10^{-10}\ m^2$	[16]
Original porosity	ϵ_0	0.6	[16]
Fluid density	ρ	$1400\ kg\ m^{-3}$	[17]
Fluid Viscosity	μ	$0.0044\ Pa\ s$	[17]

References

[1] M. Jiao, T. Liu, C. Chen, M. Yue, G. Pastel, Y. Yao, H.Xie, W. Gan, A. Gong, X. Li, L. Hu, Holey three-dimensional wood-based electrode for vanadium flow batteries. Energy Storage Materials, 27 (2020) 327-332.

[2] M.C. Ribadeneyra, L. Grogan, H. Au, P. Schlee, S. Herou, T. Neville, P. L.Cullen, M. D. R. Kok, O. Hosseinaei, S. Danielsson, P. Tomani, M. M. Titirici, D. J. L. Brett, P. R. Shearing, R. Jervis, A. B. Jorg, Lignin-derived electrospun freestanding carbons as alternative electrodes for redox flow batteries, Carbon, 157 (2020) 847-856.

[3] M. Park, Y. J. Jung, J. Kim, H. Lee, J. Cho, Synergistic effect of carbon nanofiber/nanotube composite catalyst on carbon felt electrode for high-performance all-vanadium redox flow battery, Nano Letter 13 (2013) 4833-4839.

[4] R. Wang, Y. S. Li, Twin-cocoon-derived self-standing nitrogen-oxygen-rich monolithic carbon material as the cost-effective electrode for redox flow batteries, Journal of Power Sources, 421 (2019) 139-146.

[5] M. Park, J. Ryu, Y. Kim, J. Cho, Corn protein-derived nitrogen-doped carbon materials with oxygen-rich functional groups: a highly efficient electrocatalyst for all-vanadium redox flow batteries, Energy & Environment Science, 7 (2014) 3727-3735.

[6] Y. Xiang, W. D. Daoud, Binary $NiCoO_2$-modified graphite felt as an advanced positive electrode for vanadium redox flow batteries, Journal of Materials Chemistry A, 7 (2019) 5589-5600.

[7] Q. Deng, P. Huang, W. X. Wu, Q. Ma, N. Zhou, H. Xie, W. Ling, C. J. Zhou, Y. X. Yin, X. W. Wu, X. Y. Lu, Y. G. Guo, A high-performance composite electrode for vanadium redox flow batteries, Advanced Energy Materials, 7 (2017) 1700461.

[8] S. J. Yoon, S. Kim, D. K. Kim, S. So, Y. T. Hong. R. Hempelmann, Ionic liquid derived nitrogen-doped graphite felt electrodes for vanadium redox flow batteries, Carbon, 166 (2020) 131-137.

[9] D. M. Kabtamu, J. Chen, Y. Chang, C. Wang, Electrocatalytic activity of Nb-doped hexagonal WO_3 nanowire-modified graphite felt as a positive electrode for vanadium redox flow batteries, Journal of Materials Chemistry A, 4 (2016) 11472-11480.

[10] A. W. Bayeh, D. M. Kabtamu, Y. C. Chang, G. C. Chen, H. Y. Chen, G. Y. Lin, T. R. Liu, T. H. Wondimu, K. C. Wang, C. H. Wang, Synergistic effects of a TiNb2O7–reduced grapheme oxide nanocomposite electrocatalyst for high-performance all-vanadium redox flow batteries Journal of Materials Chemistry A, 6 (2018) 13908-13917.

[11] X. W. Wu, Q. Deng, C. Peng, X. X. Zeng, A. J. Wu, C. J. Zhou, Q. Ma, Y. X. Yin, X. Y. Lu, Y. G. Guo, Unveiling the role of heteroatom gradient-distributed carbon fibers for vanadium redox flow batteries with long service life, ACS Applied Materials & Interfaces, 11 (2019) 11451-11458.

[12] P. Huang, W. Ling, H. Sheng, Y. Zhou, X. P. Wu, X. X. Zeng, X. W. Wu, Y, G, Guo, Heteroatom-doped electrodes for all-vanadium redox flow batteries with ultralong lifespan. Journal of Materials Chemistry A, 6 (2018) 41-44.

[13] H. Zhou, Y. Shen, J. Xi, X. Qiu, L. Chen, ZrO2-nanoparticle-modified graphite felt: bifunctional effects on vanadium flow batteries, ACS Applied Materials & Interfaces, 8 (2016) 15369-15378.

[14] L. Wu, Y. Shen, L. Yu, J. Xi, X. Qiu, Boosting vanadium redox flow battery performance by nitrogen-doped carbon nanospheres electrocatalyst, Nano Energy, 28 (2016) 19-28.

[15] Y. Liu, Y. Shen, L. Yu, L. Liu, F. Liang, X. Qiu, J. Xi, Holey-engineered electrodes for advanced vanadium flow batteries, Nano Energy 43 (2018) 55-62.

[16] H.R. Jiang, B.W. Zhang, J. Sun, X.Z. Fan, W. Shyy, T.S. Zhao, A gradient porous electrode with balanced transport properties and active surface areas for vanadium redox flow batteries, Journal of Power Sources 440 (2019) 227159.

[17] M. Skyllas-Kazacos, L. Cao, M. Kazacos, N. Kausar, A. Mousa, Vanadium electrolyte studies for the vanadium redox battery-A review. ChemSusChem, 9 (2016) 1521-1543.

[18] H. Li, F. Shen, W. Luo, J. Dai, X. Han, Y. Chen, Y. Yao, H. Zhu, K. Fu, E. Hitz, L. Hu, Carbonized-leaf Membrane with Anisotropic Surfaces for Sodium-ion Battery, ACS Applied Materials & Interfaces, 8 (2016) 2204-2210.

[19] Z. Zhang, T. Zhao, B. Bai, L. Zeng, L. Wei, A highly active biomass-derived electrode for all vanadium redox flow batteries, Electrochemica Acta, 248 (2017) 197-205.